Chinese Chemical Letters 35 (2024) 109932

Contents lists available at ScienceDirect

Chinese Chemical Letters

journal homepage: www.elsevier.com/locate/cclet

MOF-derived Cu based materials as highly active catalysts for improving hydrogen storage performance of Mg-Ni-La-Y alloys

Yufei Liu[a,b], Liang Xiong[c,*], Bingyang Gao[c], Qingyun Shi[a,b], Ying Wang[a], Zhiya Han[c], Zhenhua Zhang[c], Zhaowei Ma[d,*], Limin Wang[a,b], Yong Cheng[a,*]

[a] State Key Laboratory of Rare Earth Resource Utilization, Changchun Institute of Applied Chemistry, Chinese Academy of Sciences, Changchun 130022, China
[b] School of Applied Chemistry and Engineering, University of Science and Technology of China (USTC), Hefei 230026, China
[c] Purification Equipment Research Institute of CSIC, Handan 056002, China
[d] Shengyuan (Xiamen) Hydrogen Energy Research Institute Co., Ltd., Xiamen 361000, China

ARTICLE INFO

Article history:
Received 12 April 2024
Accepted 28 April 2024
Available online 29 April 2024

Keywords:
Mg-Ni-La-Y alloy
Cu@C
Catalyst
Kinetics
Hydrogen storage

ABSTRACT

Higher initial (de)hydrogenation temperature and sluggish kinetics are the main bottlenecks to develop Mg-based hydrogen storage alloys with high hydrogen capacity. One of the effective methods of solving these problems is introducing additives to enhance (de)hydrogenation kinetics and decrease particle sizes to lower (de)hydrogenation temperatures. In this work, Mg85-Ni10-La4.5-Y0.5 alloy doped with Cu@C nanoparticles is prepared, which could enhance (de)hydrogenation kinetics *via* introducing Cu nanoparticles as a catalyst and reduce the alloy particle sizes *via* acting as a grinding agent to lower (de)hydrogenation temperature. The results indicate the dehydrogenation temperature of the modified Mg85-Ni10-La4.5-Y0.5 composite could be decreased to 308.5 °C, absorb 4.73 wt% H_2 at 220 °C within 1 min and release 5.01 wt% H_2 within 4 min at 300 °C. Moreover, the capacity retention could be maintained around 98.8% after 10 cycles at 300 °C, superior than those of Mg85-Ni10-La4.5-Y0.5 and milled-Mg85-Ni10-La4.5-Y0.5. DFT results and characterizations suggest that *in-situ* formed Mg_2Cu could accelerate the dissociation of Mg-H bonds and the presence of amorphous carbon in Mg-Ni-La-Y-Cu system will further synergistically improve the (de)hydrogenation kinetics of Mg85-Ni10-La4.5-Y0.5. Reduced particle sizes under the aid of carbon frameworks also help introduce boundaries of the particles and shorten hydrogen diffusion pathways.

Solid-state hydrogen storage maybe the most promising hydrogen storage technology due to the advantages of high-volume hydrogen storage density, high safety, and long storage time [1,2]. Among current developed solid-state hydrogen storage materials, magnesium (Mg)-based metal hydride has been considered as one of efficient solid-state hydrogen storage materials due to high mass and volume hydrogen storage density (~7.6 wt%, 110 g/L), abundant resources, low price, environment-friendly [3,4]. However, there are still many problems in the practical application of Mg-based metal hydrides: (1) Higher (de)hydrogenation enthalpy and activation energy lead to high (de)hydrogenation temperature (usually above 300 °C); (2) Poor dissociation/recombination ability of H_2 molecule/H atom, and low diffusion rate of H atom leads to slow hydrogen (de)hydrogenation kinetics. (3) Mg-based metal hydride particles are easy to agglomerate/grow during (de)hydrogenation cycling, results in poor cycle stability and hydrogen storage capacity decline. How to adopt appropriate strategies to regulate the structure and compositions of Mg-based hydrogen storage materials to overcome the energy barrier in the evolution of the H atom and then improve the thermodynamic and (de)hydrogenation kinetic properties have always been hot and difficult topics. As an efficient and simple strategy, doping additives with different phases and compositions have been applied extensively to enhance the hydrogen storage properties of Mg-based alloys [5]. Over the past decades, various catalysts including transition metals (Ti, Ni, V, Co, Mn, *etc.*) [6], their corresponding oxide [7], metallic carbide [8], metallic nitride, and metallic fluoride have been intensively studied.

Generally, transition metal catalysts can dissociate H_2 molecules rapidly for hydrogen absorption and catalyze the H–H complex desorption during hydrogen release, which facilitates the kinetics of hydrogen absorption/desorption in the Mg/MgH_2 system [9,10]. Transition metal carbides and transition metal nanoparticles wrapped with carbon have better catalytic performance among

* Corresponding authors.
E-mail addresses: xiongliang_1206@163.com (L. Xiong), mazwfly@163.com (Z. Ma), cyong@ciac.ac.cn (Y. Cheng).

https://doi.org/10.1016/j.cclet.2024.109932
1001-8417/

transition metal catalysts. Fu *et al*. created a bamboo-like CNT-supported bimetallic NiFe alloy catalyst to enhance the hydrogen storage performance of the Mg/MgH_2 system [11]. The synergistic effect of the "hydrogen pumping" of Mg_2Ni/Mg_2NiH_4 and the "hydrogen channeling" of α-Fe, as well as the good dispersion of the carbon nanotubes, significantly enhance the hydrogen storage performance. Hamamelis-like $K_2Ti_6O_{13}$ was synthesized from alkali Ti_3C_2 MXene and NaOH through a hydrothermal strategy by Liu *et al*. [12], which significantly improved the hydrogen storage performance of MgH_2. The generated active substances of $KMgH_3$, Ti, and TiO are responsible for the outstanding performance. The results confirm the unique nanostructure can elevate the enhancement effect of K_2Ti6O_{13}. Two kinds of metal-organic frameworks (MOFs) based on Co(II) and Fe(II) as metal ions and trimeric acid (TMA) as organic linker were synthesized by Ma *et al*. [13]. The improvement in the sorption kinetics of the MgH_2-TM MOF (TM = Co, Fe) powders was mainly attributed to the catalytic effects of nano-sized Mg_2Co and α-Fe formed on the surface of Mg/MgH_2 particles, significantly reduced the apparent dehydrogenation activation energy from 181.4 kJ/mol (MgH_2) to 151.3 kJ/mol (MgH_2-Co MOF) and 142.3 kJ/mol (MgH_2-Fe MOF). Moreover, the carbon material is a kind of fantastic catalyst carrier, and it has the effect of providing active sites and preventing particle agglomeration in the MgH_2/Mg system [14]. Therefore, the combination of transition metal and carbon (TM@C) would be an outstanding catalyst for improving the hydrogen storage performance of Mg-based materials [15].

In this paper, a simple route to synthesize the Cu@C composite catalyst is investigated, which is cheap and stable in high temperatures. Besides, the effect of catalysts with different mass percentages on the hydrogen storage performance of Mg85-Ni10-La4.5-Y0.5 alloy is systematically measured, and the appropriate catalyst addition is selected.

As shown in Fig. 1a, the synthesis process of the Cu@C catalyst was depicted. X-ray diffraction (XRD) pattern of this precursor could be corresponded to the standard of $[Cu_3(BTC)_2]_n$ (Cu-BTC). After heat-treatment under an inert atmosphere, Cu@C composite composed of metallic Cu phase and carbon framework was obtained (Fig. 1b). According to the thermal gravimetric analyzer (TGA) result of Cu@C composite measured in an air atmosphere (Fig. 1c), shows the TGA curve of Cu@C measured in an air atmosphere, the content of Cu phase was calculated around 54.3 wt% and corresponding ratio of carbon content can be calculated to be 45.7 wt%. The chemical states on the surface of Cu@C were characterized by X-ray photoelectron spectroscopy (XPS) technique (Fig. 1d). The characteristic peaks of high-resolution of O 1s spectra at 531.8 eV can be attributed to Cu-O species (Fig. 1e). For the C 1s spectrum, the peaks at 284.6, 286.2, and 288.5 eV correspond to C-C, C-O, and O-C=O, respectively (Fig. 1f). The two characteristic peaks of two of the higher energies at 932.8 and 952.3 eV can be attributed to Cu^0 species (Fig. 1g). The other two peaks around 934.5 and 954.4 eV in the Cu 2p spectra can be attributed to Cu(II) located in the

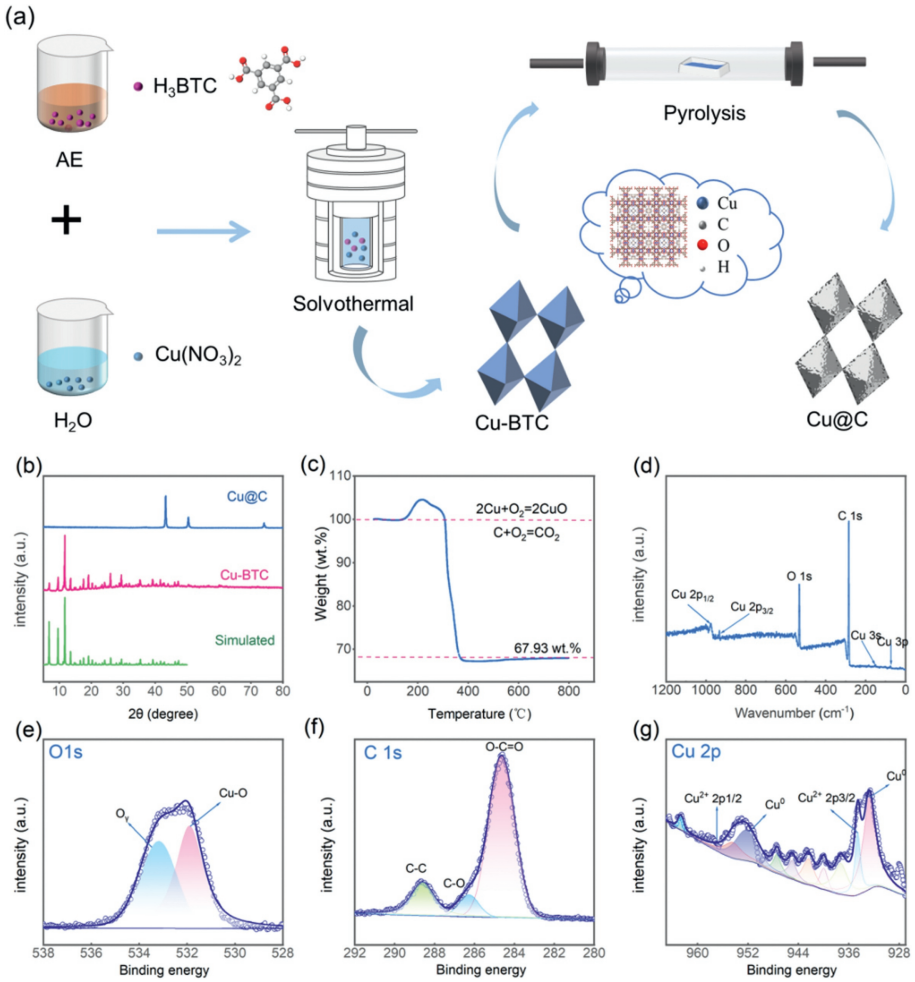

Fig. 1. The characterizations of Cu@C composite. (a) Synthesis schematic. (b) XRD patterns of Cu@C and Cu-BTC composites. (c) TGA curve. (d) XPS spectra. High-resolution XPS spectra of (e) O 1s, (f) C 1s, (g) Cu 2p.

center of the Cu@C structure, corresponding to Cu $2p_{3/2}$ and Cu $2p_{1/2}$, respectively.

The porous structure of Cu@C composite was performed by N_2 isothermal adsorption-desorption curves. According to the results of BET analysis, the surface area of Cu@C was 47.03 m^2/g and the average pore size was 3.94 nm, which verified the main mesoporous structure in the Cu@C catalyst (Figs. S1a and b in Supporting information). It was obvious that Cu@C composite with a larger defect density, which provided more catalytic active sites for the nucleation during (de)hydrogenation process and reduced the activation energy. Corresponding Raman spectrum indicated the G band around 1580 cm^{-1} attributed to sp^2 carbon atoms and the D band around 1350 cm^{-1} attributed to the defect structure inside the carbon (Fig. S1c in Supporting information). The intensity ratio of the D and G bands (I_D/I_G) reflected the graphitization degree and defect density of the carbon specimens [16]. The I_D/I_G of Cu@C was 1.11, which reflected Cu@C with a greater defect density. In addition, the high-resolution transmission electron microscope (TEM) image in Fig. S2a (Supporting information) showed that a carbon film adheres to the surface of the particles after heat treatment. Cu@C particles also could be identified by the SAED pattern (Fig. S2c in Supporting information), the results were consistent with the XRD results. Typical HAADF-STEM image of the Cu@C composite showed the inner bright region of the Cu element can be utterly encapsulated in the outer dark region of the C element (Fig. S2d in Supporting information), which was further confirmed by the EDX mappings (Figs. S2e–h in Supporting information). It could be seen from Fig. S3a (in Supporting information) that the hydrogen absorption rate increased at the initial stage and then decreased with the increase of catalyst content. As can be seen from Fig. S3b (Supporting information), the hydrogen release rate of Mg85-Ni10-La4.5-Y0.5-15 wt% Cu@C was the fastest in the early stages, but slower than that of Mg85-Ni10-La4.5-Y0.5-10 wt% Cu@C in the later stage. Therefore, 10 wt% of Cu@C doped with Mg85-Ni10-La4.5-Y0.5 maybe considerable for the overall (de)hydrogenation performances.

To characterize the kinetics at different temperatures, isothermal (de)hydrogenation performances of alloys were measured after sufficient activation. And corresponding hydrogenation kinetics curves were displayed in Figs. 2a and b under the original pressure of 5 MPa at 220 and 240 °C, respectively. As shown in Fig. 2a, the onset hydrogen desorption rate of Mg85-Ni10-La4.5-Y0.5-10 wt% Cu@C composite at 220 °C was 4.73 wt% within a minute, slightly more superior than that of milled-Mg85-Ni10-La4.5-Y0.5 (2.67 wt%). Higher hydrogen absorption capacity and kinetics at lower temperatures indicated better catalytic activity of Cu@C composite.

To further explore the hydrogenation reaction mechanism of Mg85-Ni10-La4.5-Y0.5-10 wt% Cu@C, the Johnson-Mehl-Avrami (JMAK) equation was used to study the hydrogenation kinetics systematically [17], and the JMAK model defined solid-state phase transition as three simultaneous processes, including nucleation, growth, and impingent, where the equation can be described as follows:

$$\left[-\ln(1-\alpha)\right]^{1/n} = kt \tag{1}$$

$$\ln\left[-\ln(1-\alpha)\right] = n\ln k + n\ln t \tag{2}$$

where t stands for the reaction time, α corresponds to the reaction conversion, k represents the reaction rate constant and n is the Avrami index. The nucleation and growth mechanism during hydrogenation can be speculated by the reaction order. The isothermal hydrogenation curves presented different stages, where each stage exhibited different Avrami exponents and rate constants. At 220 °C (Fig. 2c), the n value for milled-Mg85-Ni10-La4.5-Y0.5 ($n = 0.91$) was close to 1, which indicated that the initial hydrogenation stage (<20 s) was an interface-controlled one-dimensional nucleation growth process, and H_2 was absorbed on the surface of the bulk. With the progress of the hydrogenation reaction, the milled-Mg85-Ni10-La4.5-Y0.5 belonged to the one-dimensional nucleation growth process controlled by the diffusion rate ($n = 0.48 \approx 0.5$). Finally, the nucleation and growth mechanism of milled-Mg85-Ni10-La4.5-Y0.5 was diffusion-controlled from one-dimensional to two-dimensional growth ($n = 2.06 \approx 2$), which showed the disadvantage of its slow kinetics. The addition of Cu@C changed the growth mechanism, from the diffusion-controlled to interface-controlled step ($n = 0.83 \approx 1$), which suggested that the existence of a transition metal catalyst can greatly accelerate the diffusion process of H, and reach the saturation of hydrogen absorption [11].

The dehydrogenation curves of as-milled samples were displayed in Figs. 2d and e under the original pressure of 0.003 MPa at 260, and 280 °C, respectively. As shown in Figs. 2d and e,

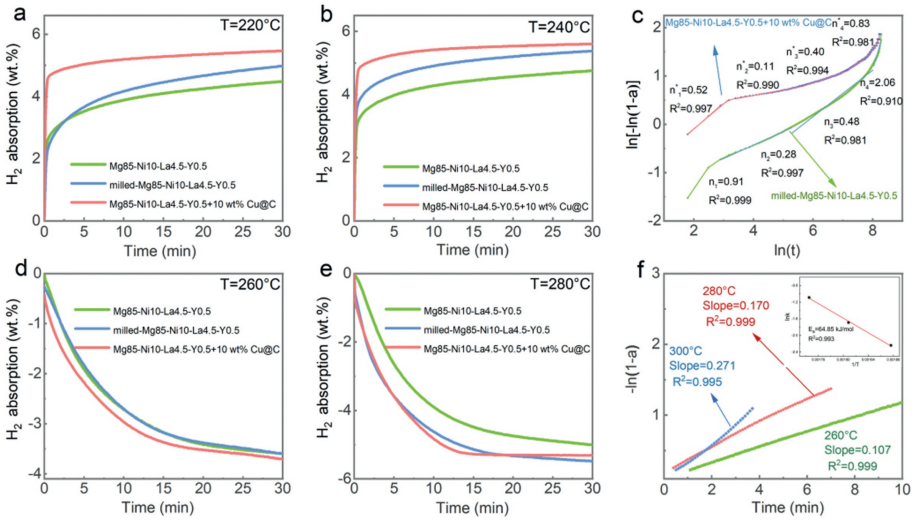

Fig. 2. Isothermal absorption kinetic curves of Mg85-Ni10-La4.5-Y0.5, milled-Mg85-Ni10-La4.5-Y0.5 and Mg85-Ni10-La4.5-Y0.5-10 wt% Cu@C at various temperature: (a) 220 °C; (b) 240 °C. (c) JMAK fitting curves of isothermal hydrogenation of Mg85-Ni10-La4.5-Y0.5-10 wt% Cu@C and milled-Mg85-Ni10-La4.5-Y0.5 at 220 °C. Isothermal desorption kinetic curves at various temperatures: (d) 260 °C; (e) 280 °C. (f) Fitting curves of the isothermal dehydrogenation curves by using JMAK.

Table 1
Comparison of the hydrogen storage property of magnesium alloy doping with different catalysts.

Various samples	Hydrogen absorption	Hydrogen desorption	E_a(abs) (kJ/mol)	E_a(des) (kJ/mol)	Ref.
$Mg_{91}Al_5Y_4$ + 5 wt% Fe@C	150 °C-2.9 wt%–150 min	300 °C-5.9 wt%–58 min	/	86.9	[19]
$Mg_{91}Al_5Y_4$ + 5 wt% Cu@C	150 °C-2.5 wt%–150 min	300 °C-5.5 wt%–200 min	/	101.9	[19]
MgH_2-Co MOF	300 °C-3.5 wt%–7200 s	/	73.9	151.3	[13]
MgH_2-Fe MOF	300 °C-3.0 wt%–1000 s	/	66.8	142.3	[13]
$Mg_{90}Al_{10}$ + 8 wt% (80 wt% Ni@Gn)	250 °C-5.1 wt%–400 s	300 °C-5.8 wt%–180 s	/	76.4	[20]
$Mg_{90}Ce_5Y_5$ + 10 wt% Co@C	200 °C-4.0 wt%–12.5 min	280 °C-4.5 wt%–40 min	/	81.9	[21]
Mg85-Ni10-La4.5-Y0.5–10 wt% Cu@C	240 °C-4.8 wt%–36 s	280 °C-5.2 wt%–816 s	/	64.9	This work

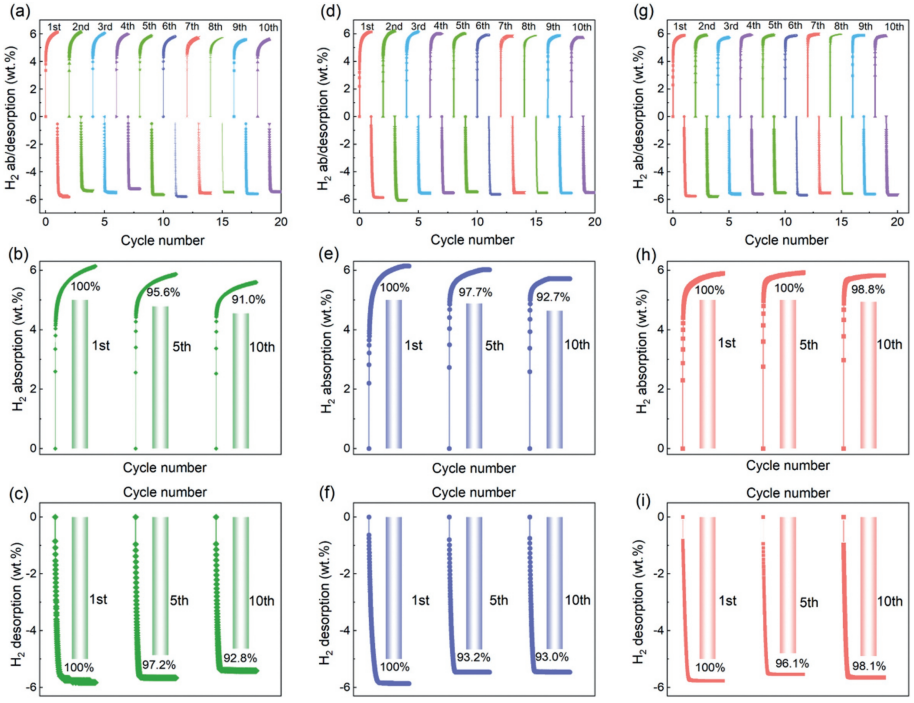

Fig. 3. Cycle performance of (a-c) Mg85-Ni10-La4.5-Y0.5 at 300 °C, (d-f) milled-Mg85-Ni10-La4.5-Y0.5, (g-i) Mg85-Ni10-La4.5-Y0.5+10 wt% Cu@C.

compared with milled-Mg85-Ni10-La4.5-Y0.5, both the dehydrogenation capacity and rate of the composites have been significantly improved for Mg85-Ni10-La4.5-Y0.5-10 wt% Cu@C at 260 and 280 °C. The isothermal method was used to calculate the apparent activation energy of Mg85-Ni10-La4.5-Y0.5 dehydrogenation, the reaction rate constant k can be obtained by linear fitting the [-ln(1 - α)] corresponding to the dehydrogenation curve at different temperatures with time (t). Herein, two theoretical models were comparatively studied to investigate the dehydriding behavior of the material, *i.e.*, the JMAK model and the contracting volume (CV) model [18], as listed in Table S1 (Supporting information). The fitting results of JMAK and CV were shown in Fig. S4 (Supporting information). Obviously, JMAK 1D presented the best linear behavior among these 6 models for the dehydrogenation reaction of the Mg85-Ni10-La4.5-Y0.5. After the values of k were calculated by JMAK 1D, the activation energy was calculated using the Arrhenius equation as follows:

$$\ln k = -\frac{E_a}{RT} + \ln A \quad (3)$$

where E_a denotes the activation energy of the dehydrogenation reaction, A means the pre-exponential factor, R signifies the universal gas constant, and T stands for the temperature of the dehydrogenation reaction. While ln$k$ and 1/T were linearly related in the Arrhenius equation. According to the Arrhenius formula, a plot between the logarithm of the reaction rate constant (ln$k$) and the inverse of the exothermic temperature (1/T) can be derived according to Fig. 2f. By linearly fitting the data points in Fig. 2f, the activation energy (E_a) of the alloy hydrogen release reaction can be obtained, and the result was shown in Fig. S5 (Supporting information), the addition of a catalyst reduced the dehydrogenation activation energy from 90.42 kJ/mol to 64.85 kJ/mol. The DSC results (Fig. S6 in Supporting information) showed a positive effect of introducing Cu@C on lowering the dehydrogenation temperature of Mg85-Ni10-La4.5-Y0.5. The peak temperature of hydrogen discharge was reduced from 381.7 °C to 308.5 °C. Besides, the hydrogen storage property of magnesium alloy doped with other MOFs and catalysts were compared with Mg85-Ni10-La4.5-Y0.5–10 wt% Cu@C here in Table 1 [13,19–21]. Among these composites, Mg85-Ni10-La4.5-Y0.5–10 wt% Cu@C showed the lowest de/hydrogenation kinetic barriers, further indicating a good catalytic activity of Cu@C composite.

Cycling stability is also a key factor for the practical application of hydrogen storage materials. The cyclic stability of samples was tested at a relatively high temperature of 300 °C (Fig. 3). The attenuation of Mg85-Ni10-La4.5-Y0.5–10 wt% Cu@C was undetectable after 5 cycles. In contrast, the retention rate of hydrogen absorption capacity of Mg85-Ni10-La4.5-Y0.5 and milled-Mg85-Ni10-La4.5-Y0.5 was reduced to 95.6% and 97.7%. Furthermore, the hydrogen desorption kinetics of Mg85-Ni10-La4.5-Y0.5–10 wt% Cu@C at 300 °C maintains at a high level after 10 cycles and the hydrogen content was sustained at 5.65 wt% with a hydrogen capacity retention of 98.1%, was much higher than that of Mg85-Ni10-La4.5-Y0.5 (92.8%) and ball-milled Mg85-Ni10-La4.5-Y0.5

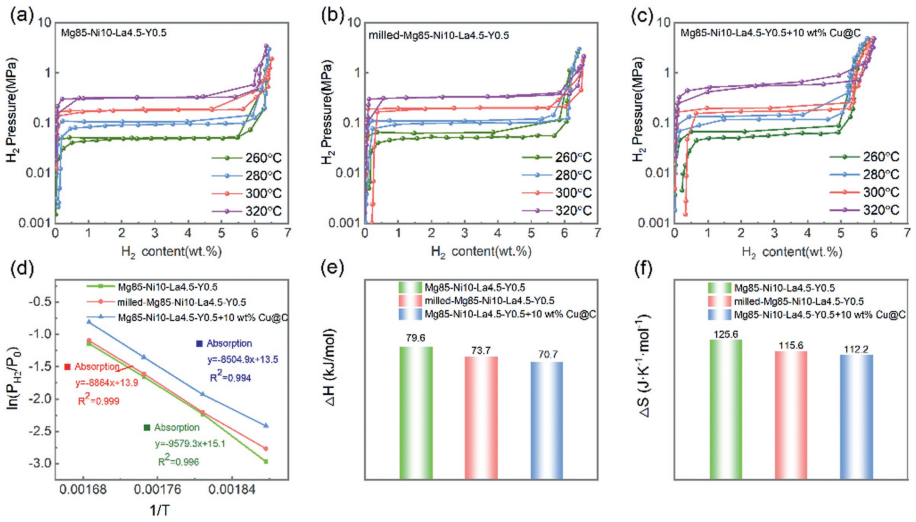

Fig. 4. PCT curves of (a) Mg85-Ni10-La4.5-Y0.5, (b) milled-Mg85-Ni10-La4.5-Y0.5, (c) Mg85-Ni10-La4.5-Y0.5-10 wt% Cu@C. (d) Van't Hoff plots for the hydrogen absorption and desorption process. (e) Enthalpy change of the hydrogen absorption reaction. (f) Entropy change of the hydrogen absorption reaction.

(93.0%). The better cycling capability of Mg85-Ni10-La4.5-Y0.5–10 wt% Cu@C can be attributed to the outstanding catalytic effect of Cu@C during the hydrogen absorption/desorption process [22,23]. In addition, copper has stable physical and chemical properties and good thermal conductivity, so copper catalysts have a long service life and can be used for a long time under high temperatures and pressure without losing activity, this meets the conditions for high-temperature hydrogen ab/desorption in Mg-based materials.

Thermodynamics properties were carried out by utilizing the PCT apparatus, as inserted in Fig. 4, from which the enthalpy change (ΔH) and entropy change (ΔS) are obtained according to the following Van't Hoff equation:

$$ln\frac{P_{H_2}}{P_0} = \frac{\triangle H}{RT} - \frac{\triangle S}{R} \tag{4}$$

In this equation, ΔH stands for the enthalpy change; ΔS represents the entropy change; R signifies the gas constant; P_{H_2} means the hydrogen pressure; P_0 stands for the standard atmospheric pressure, and T is the absolute temperature. Based on the linear relation between ln (P_{H_2}/P_0) and $1/T$ [24], the stability of a metal hydride can be determined from the magnitude of the ΔH value. The larger of ΔH indicates the metal hydride is more stable and is less likely to undergo hydrogen evolution. Entropy change refers to the decomposition extent of the hydride, the larger value of ΔS indicates the reaction is less likely to occur. Ball-milling can reduce the enthalpy change of the hydrogen absorption reaction from 79.6 kJ/mol to 73.7 kJ/mol and the entropy change of the hydrogen absorption reaction from 125.6 JK^{-1} mol^{-1} to 115.6 JK^{-1} mol^{-1}. The enthalpy changes of Mg85-Ni10-La4.5-Y0.5–10 wt% Cu@C during hydrogen absorption was 70.7 kJ/mol, and entropy change was 112.2 JK^{-1} mol^{-1}, respectively. The inclusion of catalysts facilitates the improvement of thermodynamic properties. In addition, the increase of Cu@C can also cause the decreased hydrogen absorption capacity from 6.57 wt% to 5.74 wt%, which was due to the role of Cu@C as a catalyst rather than hydrogen absorption active material.

Fig. 5a demonstrated the XRD patterns of alloys before hydrogen absorption, all the composites showed similar peak shapes, which indicated that the samples share a similar phase composition and crystal structure. Furthermore, the composites were comprised of the main phase of Mg (PDF #89-5003), the minor phase of Mg_2Ni (PDF #65-9357), La_2Mg_{17} phase (PDF #65-3648) [25]. The weak Cu diffraction peak located at 43.3° indicated that the Mg85-Ni10-La4.5-Y0.5-10 wt% Cu@C composite was successfully synthesized. The new carbide or Cu-based crystal phase was undetectable, suggesting that the composite was just mechanical mixing. It is worth mentioning that the zero-valent copper and Mg have not formed Mg-Cu intermetallic during ball milling due to the covered action of the thin carbon layers on the Cu nanoparticles. Fig. 5b showed the XRD patterns of the hydrogenated Mg85-Ni10-La4.5-Y0.5-10 wt% Cu@C, in this process, hydrogen reacted with alloys as follows:

$$Mg + H_2 \leftrightarrow MgH_2 \tag{5}$$

$$Mg_2Ni + H_2 \leftrightarrow Mg_2NiH_4 \tag{6}$$

$$La_2Mg_{17} + H_2 \rightarrow LaH_3 + MgH_2 \tag{7}$$

$$MgH_2 + Cu \leftrightarrow MgCu_2 + H_2 \tag{8}$$

$$MgH_2 + MgCu_2 \leftrightarrow Mg_2Cu + H_2 \tag{9}$$

The diffraction peaks of MgH_2 and Mg_2NiH_4 completely disappeared after hydrogen release and consist of the Mg_2Ni, Mg, and H_2 phases, indicating that MgH_2 and Mg_2NiH_4 were completely decomposed into Mg and Mg_2Ni (Fig. 5c). In the initial stage of hydrogen release, Mg_2NiH_4 firstly releases hydrogen to produce Mg_2Ni, after which the surrounding MgH_2 continuously transfers H atoms to Mg_2Ni and continues to release hydrogen. Therefore, the role of Mg_2Ni/Mg_2NiH_4 is to act as the active site, and it is easier for MgH_2 to release hydrogen through the active site than to release hydrogen directly [26]. La_2Mg_{17} absorbs hydrogen to form LaH_3 and MgH_2, but rare earth hydrides have a high hydrogen release temperature and do not dehydrogenate under experimental temperature conditions [27]. Rare earth [28] elements in the hydrogen absorption process will be converted into high-stability rare earth hydrides, For instance, the *in situ* generated LaH_3 increases the number of grain boundaries and phase boundaries [29], which provides favorable conditions for the diffusion of hydrogen and the nucleation and growth of Mg/MgH_2, thus improving the rate of hydrogen absorption and discharge. Amorphous carbon loaded Cu adheres to the surface of the Mg85-Ni10-La4.5-Y0.5 catalyst system under ball-milling, which not only acts as an effective dispersion medium of the catalysts, making them full contact with Mg85-Ni10-La4.5-Y0.5 and undergo *in situ* transformation, but also

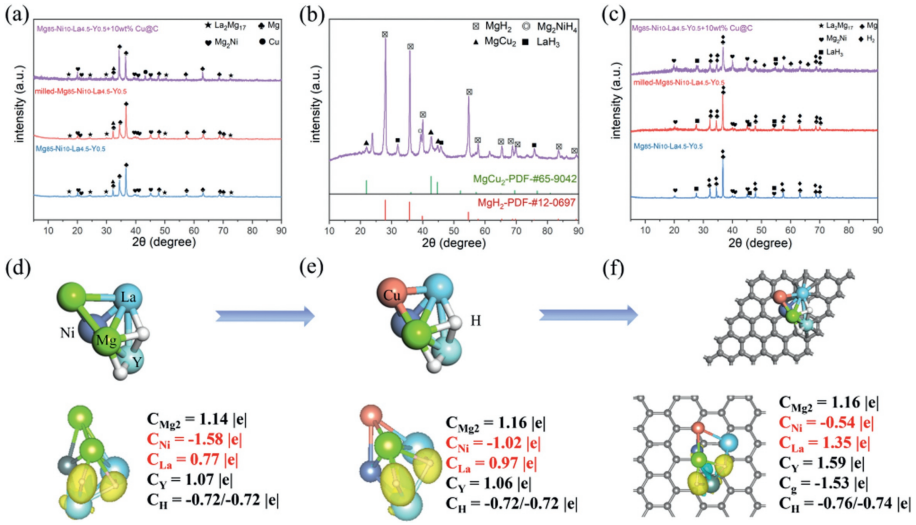

Fig. 5. (a) XRD patterns of Mg85-Ni10-La4.5-Y0.5, milled-Mg85-Ni10-La4.5-Y0.5, and Mg85-Ni10-La4.5-Y0.5-10 wt% Cu@C. (b) XRD patterns of hydrogenated Mg85-Ni10-La4.5-Y0.5-10 wt% Cu@C. (c) XRD patterns of dehydrogenated alloys. (d) The optimized structures of Mg-Ni-La-Y and charge density difference. (e) The optimized structures of Mg-Ni-La-Y with Cu and charge density difference. (f) The optimized structures of Mg-Ni-La-Y with Cu@C and charge density difference.

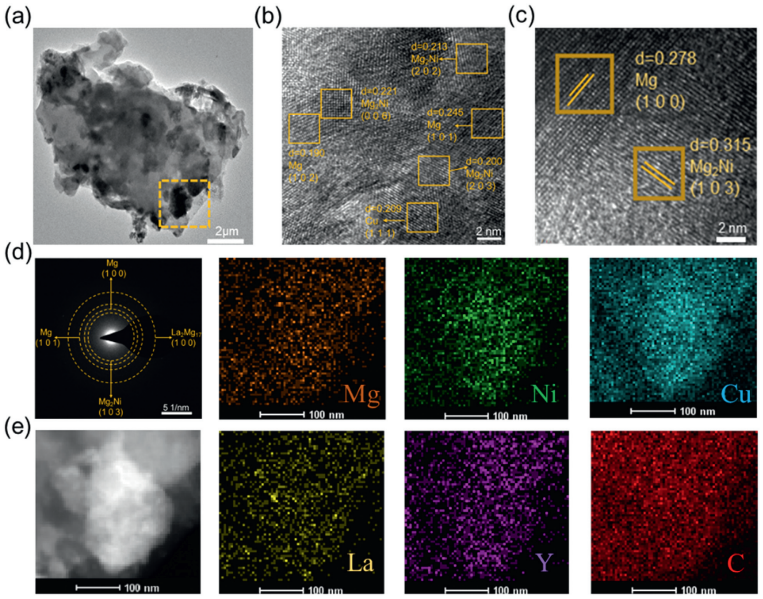

Fig. 6. (a) TEM of Mg85-Ni10-La4.5-Y0.5-10 wt% Cu@C. (b, c) The detailed HRTEM image. (d) SAED pattern of Mg85-Ni10-La4.5-Y0.5-10 wt% Cu@C. (e) STEM-BF image and corresponding EDX mappings of Mg, Ni, La, Y, Cu, and C.

effectively disperse the entire hydrogen storage system, greatly reducing the agglomeration of particles. During the hydrogen absorption and desorption process, MgH_2 reacted with copper to generate nano $MgCu_2$ and Mg_2Cu *in situ*, and Mg_2Cu was considered to accelerate the dissociation of hydrogen molecules and promoted the hydrogenation of the Mg phase, playing a significant catalytic role in the formation of the MgH_2 phase [24,30,31]. First principal calculations were carried out to investigate the synergistically catalytic mechanism of Mg85-Ni10-La4.5-Y0.5-Cu@C system. The charge density difference of the Mg-Ni-La-Y cluster, Mg-Ni-La-Y cluster interacting with Cu (111) and C coating Cu (111) were presented in Figs. 5d–f. Due to the weaker electronegativity of Mg (1.31) compared to Cu (1.90), after the reaction between Mg and Cu to form Mg_2Cu, the charge undergoes redistribution (the red charge changes significantly), resulting in a change in the bond energy between H and the metal and then the longest Mg-H bond length increased from 2.23 Å to 2.24 Å (Figs. 5d and e). As shown in Fig. 5f, it was found that there was more charge transfer between catalysts and the Mg-Ni-La-Y cluster when carbon was loaded with Cu, indicating the enhanced chemical activity by carbon coating. This charge transfer also enhances the electron localization on H atoms in the Mg-Ni-La-Y-Cu@C system, thus can further lead to the weakening of Mg-H bonding remarkably, the longest Mg-H bond length increased from 2.24 Å to 2.26 Å [32]. Therefore, the presence of amorphous carbon in Mg-Ni-La-Y-Cu@C system will further synergistically improve the dehydrogenation kinetics of Mg85-Ni10-La4.5-Y0.5, according to the first principal calculation results [33–37].

TEM observations were conducted in Fig. 6 to further reveal the morphology of Mg85-Ni10-La4.5-Y0.5-10 wt% Cu@C, two of the interplanar spacings of the selected zones in Fig. 6b can be determined to be about 0.200 and 0.213 nm, which were nearly iden-

tical to that of Mg_2Ni (203) and (202) plane. Similarly, Mg (101) plane La_2Mg_{17} (304) and Cu (111) plane with interplanar spacings of 0.245, 0.211, and 0.209 nm can also be confirmed in Fig. 6b. At the same time, the SAED pattern in Fig. 6d for Mg85-Ni10-La4.5-Y0.5-10 wt% Cu@C can be indexed with (101), and (100) for Mg, (103) for Mg_2Ni and (304) for La_2Mg_{17}. The EDX results (Fig. 6e) indicated that the element distribution was uniform, and under the mechanical action of ball milling, the catalyst uniformly covered the surface of the alloy and served to refine the particles and the addition of catalysts with a high degree of defects provided more catalytically active sites for the nucleation of the absorption/desorption process and reduces the activation energy.

The finer the particle size of the material, the more favorable the rate of hydrogen absorption release. The boundaries of the particles are more likely to be the sites of hydride formation and dissociation. Therefore, the finer the particles, the more corresponding particle boundaries and the more favorable the hydrogen absorption/release reaction will be. The smaller the particle size of the material, the shorter the diffusion path of hydrogen in the material and the more favorable the hydrogen absorption/release reaction is. According to Fig. S7 (Supporting information), the addition of Cu@C helpd to reduce the particle size, which enhanced the hydrogen absorption and discharge kinetics of the composite.

In conclusion, the carbon-loaded transition metal catalyst (Cu@C) is obtained by a simple solvothermal and heat treatment process. It has an excellent catalyst effect on improving the hydrogen storage performance of Mg-based materials. The Mg85-Ni10-La4.5-Y0.5-10 wt% Cu@C composite exhibits excellent performance in both hydrogenation and dehydrogenation, the kinetic performance had been improved and the peak hydrogen release temperature had also been reduced markedly. The DFT calculation shows that there is a strong charge transfer between Mg-Ni-La-Y and Cu@C, which results in changing the charge distribution of Mg and H, weakening the Mg-H bond, and reducing the stability of MgH_2. In conclusion, a new idea for the construction of multi-phase and multi-scale hydrogen storage systems is provided by the combination of transition metals and carbon materials.

Declaration of competing interest

The authors declare that they have no known competing financial interests or personal relationships that could have appeared to influence the work reported in this paper.

CRediT authorship contribution statement

Yufei Liu: Writing – original draft. **Liang Xiong:** Writing – review & editing. **Bingyang Gao:** Funding acquisition. **Qingyun Shi:** Writing – review & editing. **Ying Wang:** Writing – review & editing. **Zhiya Han:** Funding acquisition. **Zhenhua Zhang:** Funding acquisition. **Zhaowei Ma:** Funding acquisition. **Limin Wang:** Writing – review & editing. **Yong Cheng:** Writing – review & editing.

Acknowledgments

This study was funded by National Key R&D Program of China (No. 2021YFB4000604), the National Natural Science Foundations of China (No. 52261041), Key R&D projects of Jilin Provincial Science and Technology Development Plan (No. 20230201125GX), Youth Growth Science and Technology Program of Jilin Province (No. 20220508001RC), Youth Innovation Promotion Association CAS (No. 2022225), Independent Research Project of the State Key Laboratory of Rare Earth Resources Utilization, and Changchun Institute of Applied Chemistry, Chinese Academy of Sciences (No. 110000RL86).

Supplementary materials

Supplementary material associated with this article can be found, in the online version, at doi:10.1016/j.cclet.2024.109932.

References

[1] Z. Chen, Z. Ma, J. Zheng, et al., Chin. J. Chem. Eng. 29 (2021) 1–12.
[2] A. Kumar, P. Muthukumar, P. Sharma, E.A. Kumar, Sustain. Energy Technol. Assess. 52 (2022) 102204.
[3] I.P. Jain, C. Lal, A. Jain, Int. J. Hydrog. Energy 35 (2010) 5133–5144.
[4] H. Shao, L. He, H. Lin, H.W. Li, Energy Technol. 6 (2017) 445–458.
[5] Y. Yang, X. Zhang, L. Zhang, et al., J. Mater. Sci. Technol. 163 (2023) 182–211.
[6] M. Pozzo, D. Alfè, Int. J. Hydrog. Energy 34 (2009) 1922–1930.
[7] W. Oelerich, T. Klassen, R.J.J.O.A. Bormann, J. Alloy. Compd. 315 (2001) 237–242.
[8] Z. Tian, Z. Wang, P. Yao, et al., Int. J. Hydrog. Energy 46 (2021) 40203–40216.
[9] J. Zhang, S. Yan, L.P. Yu, et al., Int. J. Hydrog. Energy 43 (2018) 21864–21873.
[10] J. Zhang, S. Yan, G. Xia, et al., J. Magnes. Alloy. 9 (2021) 647–657.
[11] Y. Fu, Z. Yu, S. Guo, et al., Chem. Eng. J. 458 (2023) 141337.
[12] Q. Kong, H. Zhang, Z. Yuan, et al., ACS Sustain. Chem. Eng. 8 (2020) 4755–4763.
[13] Z. Ma, J. Zou, D. Khan, et al., J. Mater. Sci. Technol. 35 (2019) 2132–2143.
[14] L. Zhang, C. Zhao, F. Wu, Y. Wang, J. Alloy. Compd. 952 (2023) 170002.
[15] D. Feng, D. Zhou, Z. Zhao, et al., Int. J. Hydrog. Energy 46 (2021) 33468–33485.
[16] Y. Lv, M. Han, W. Gong, et al., Angew. Chem. Int. Ed. 59 (2020) 23521–23526.
[17] Y. Zhao, Y. Zhu, J. Liu, et al., J. Alloy. Compd. 862 (2021) 158004.
[18] B. Liu, B. Zhang, X. Chen, et al., Mater. Today Nano 17 (2022) 100168.
[19] X. Wei, C. Li, Q. Ge, et al., J. Alloy. Compd. 929 (2022) 167317.
[20] H.X. Huang, J.G. Yuan, B. Zhang, et al., Int. J. Hydrog. Energy 45 (2020) 798–808.
[21] H. Yong, X. Wei, J. Hu, et al., J. Magnes. Alloy. 9 (2021) 1977–1988.
[22] S. Zheng, Y. Ru, H. Xue, H. Pang, Chin. Chem. Lett. 32 (2021) 3817–3820.
[23] K. Zhang, Y. Chang, J. Lei, et al., J. Magnes. Alloy. (2023), doi:10.1016/j.jma.2023.01.020.
[24] S. Luo, S. Li, Y. Liu, et al., J. Alloy. Compd. 806 (2019) 370–377.
[25] Z.Y. Li, S.L. Li, Z.M. Yuan, Y.H. Zhang, Acta Metall. Sin. 32 (2019) 961–971.
[26] C. Zheng, D. Zhou, D. Feng, et al., J. Phys. Chem. Solids 178 (2023) 111320.
[27] D.K. Slattery, Int. J. Hydrog. Energy 20 (1995) 971–973.
[28] S. Gao, S. Zhang, Y. Li, et al., Appl. Surf. Sci. 614 (2023) 156243.
[29] F. Guo, T. Zhang, L. Shi, L. Song, Int. J. Hydrog. Energy 45 (2020) 32221–32233.
[30] C. Xu, H.J. Lin, Y. Wang, et al., J. Alloy. Compd. 782 (2019) 242–250.
[31] Y.S. Au, M. Ponthieu, R. van Zwienen, et al., J. Mater. Chem. A 1 (34) (2013) 9983–9991.
[32] M. Zhang, X. Xiao, J. Mao, et al., Mater. Today Energy 12 (2019) 146–154.
[33] K. Dutta, P. Mandal, K. Ramakrishna, O.N. Srivastava, Int. J. Hydrog. Energy 19 (1994) 253–257.
[34] G. Kresse, J.J.P.R.B. Furthmüller, Phys. Rev. B 54 (1996) 11169.
[35] G. Kresse, J.J.P.R.B. Hafner, Phys. Rev. B 47 (1993) 558.
[36] G. Kresse, D.J.P.R.B. Joubert, Phys. Rev. B 59 (1999) 1758.
[37] G.J. Kresse, Phys. Rev. B 64 (2001) 155323.